Proceedings of Engineering and Technology Innovation, vol. 27, 2024, pp. 66-83

Quantitative Shaking Evaluation of Bracing-Strengthened and Base-Isolated Buildings Using Seismic Intensity Level

Henda Febrian Egatama[1,2,*], Nanang Gunawan Wariyatno[3], Han Ay Lie[1],
Muhammad Zulfikar Adhi Muliawan[1], Buntara Sthenly Gan[4]

[1]Department of Civil Engineering, Diponegoro University, Semarang, Indonesia/ [2]Department of Civil Engineering, Atma Jaya University of Yogyakarta, Sleman, Indonesia

[3]Department of Civil Engineering, Jenderal Soedirman University, Purbalingga, Indonesia

[4]Department of Architecture, College of Engineering, Nihon University, Fukushima, Japan

Received 14 April 2024; received in revised form 24 June 2024; accepted 25 June 2024

DOI: https://doi.org/10.46604/peti.2024.13578

Abstract

In current design practice, the seismic strength design of buildings is commonly based on the strength concept, lacking a quantitative evaluation tool that can show the performance of the buildings during earthquakes. This paper demonstrates the application of seismic intensity level (SIL) as a quantitative evaluation tool for aseismic building performance. A simulation test is conducted on three categories of building-frame: non-strengthened (NA), bracing-strengthened (BS), and base-isolated (BI), subjected to a north-south (N-S) 1940 El Centro seismic wave. The criteria evaluated include maximum acceleration, energy dissipation, and the measured seismic intensity level (m-SIL). The effect of strengthening methods is compared based on those criteria. The results show that despite the apparent reduction in structural response metrics, the SIL value diminishes more substantially for base isolators (4.5 level decrease) than bracing (0.4 level decrease). This confirms that SIL provides higher consistency results and is straightforward to comprehend.

Keywords: seismic intensity level (SIL), comfort-based, shaking performance, base-isolated, earthquake

1. Introduction

Earthquake phenomena, arising from the sudden release of energy due to the movement of the Earth's crust, generate ground motions of varying intensities and frequencies. These ground motions induce forces that can cause deformations, damage, and collapse of buildings. The design and construction materials of a building influence its response to seismic force and the effectiveness of methods employed to enhance seismic resilience [1]. Understanding the interaction between seismic forces and building structures is critical, particularly for developing seismic design and building strengthening strategies aimed at protecting human life and minimizing property damage [2-3].

In response to the effects of earthquakes on buildings, El Ouni et al. [4] conducted a study of building strengthening methods, including passive and active control. Based on this study, regarding the cost-effectiveness and ease of maintenance, the most used methods are the tuned mass damper (TMD), tuned liquid damper (TLD), and bracing systems. Another study found that the base-isolation (BI) method is ineffective for near-field earthquakes [5]. The non-linear behavior of BI frame structures has been assessed using pushover analysis [6] and fragility analysis [7]. The seismic demands investigated in these studies include maximum inter-story drift, base shear, and isolator displacement. Additionally, Bhandari et al. [8] conclude

* Corresponding author. E-mail address: henda.egatama@uajy.ac.id

English language proofreader: Yen-Chun Hsieh

that the capacity spectrum method (CSM) can predict seismic demands up to a specific performance point. Abdeddaim et al. [9] conducted an advanced study aimed at improving the performance of the BI building, which demonstrated significant dynamic response enhancement using the magnetorheological (MR) damper. Furthermore, the prediction of the structural seismic response has been advanced using an artificial intelligence-based technology [10].

The practice of regularly updating seismic design codes to enhance the strength of building structures against stronger earthquakes is ongoing [11-12]. However, to effectively mitigate the impact of earthquakes, it is important to adopt a new seismic design method that reduces shaking during earthquakes in addition to the current codes. The conventional seismic design codes primarily focus on the "strength" factor. When various strengthening options are considered, the most economically favorable method is often selected, rather than one based on other criteria. Incorporating the concept of "comfort" into existing seismic design codes is recommended, as it assesses the amount of shaking a building experiences [13]. Using seismic intensity level (SIL) values as an additional design criterion in the codes would be beneficial for determining the optimal solution from various strengthening methods [14]. In addition, it is also used for disaster evaluation, as previously reported [15-17].

This paper presents a comprehensive design philosophy for evaluating earthquake-induced vibrations. It utilizes the Japan Meteorological Agency (JMA) equations to determine SIL and identify measures to minimize the risk of human casualties. The SIL values are calculated using real-time ground motion information recorded at seismic monitoring stations during earthquakes. This study aims to demonstrate the application of SIL as an evaluation tool for the seismic aspect of a building. SIL values were used to identify the most suitable strengthening method for existing buildings. The proposed selection process is based on a quantitative approach, which has not yet been incorporated into current seismic design codes. More details on the SIL and the calculation of JMA SIL can be found in Wariyatno et al. [18].

2. Materials and Methods

The calculated seismic intensity level (m-SIL) of three steel frame building categories was evaluated. The unbraced structure is denoted as NA, the braced structure is denoted as BS, and the structure with the base isolator is denoted as BI. As for the BS, ten variations of bracing configurations controlled by four variations in weight-to-building bracing ratios were investigated. The four bracing weight ratio variations were 9.5%, 16.3%, 18.9%, and 32.6% to the frame. All bracings were single or double-crossed diagonal bracings in the line of earthquake load response and identical for all floors. The building had five floors and three frames. The beam-to-column connections were fully restrained. The bracings were alternatively situated between two or three frames. The BI structure had six base isolator's mechanical property variations, including stiffness (k_{BI}), damping (c_b), and frequency ratio (ω_b/ω). Additionally, the response accelerations and kinetic energy were compared, and the floor response's influence on the SIL was analyzed.

To obtain the shaking performance of a building, the seismic wave recordings from earthquake monitoring stations were transformed from the time-domain to frequency-domain signals. The filters [19] were applied to the frequency domain of the three-component accelerations (north-south, east-west, and up-down directions) of the seismic waves from an earthquake. Once the filters had been applied, the three acceleration directions in the frequency domain were converted back to the time domain. The acceleration was then calculated using the normalized combined result of the three acceleration components as outlined in Wariyatno et al. [18].

The building prototype was a 5-story steel frame building, the details of which are presented in Fig. 1. The building conformed to Japan's seismic codes [20]. A test was conducted on the actual size of the building in the E-Defense project in Japan [20]. No bracing or base isolation in the structure and the specimen was denoted as NA. Bracings and base isolators were placed for the BS and BI specimens, and the m-SIL results were compared and contemplated.

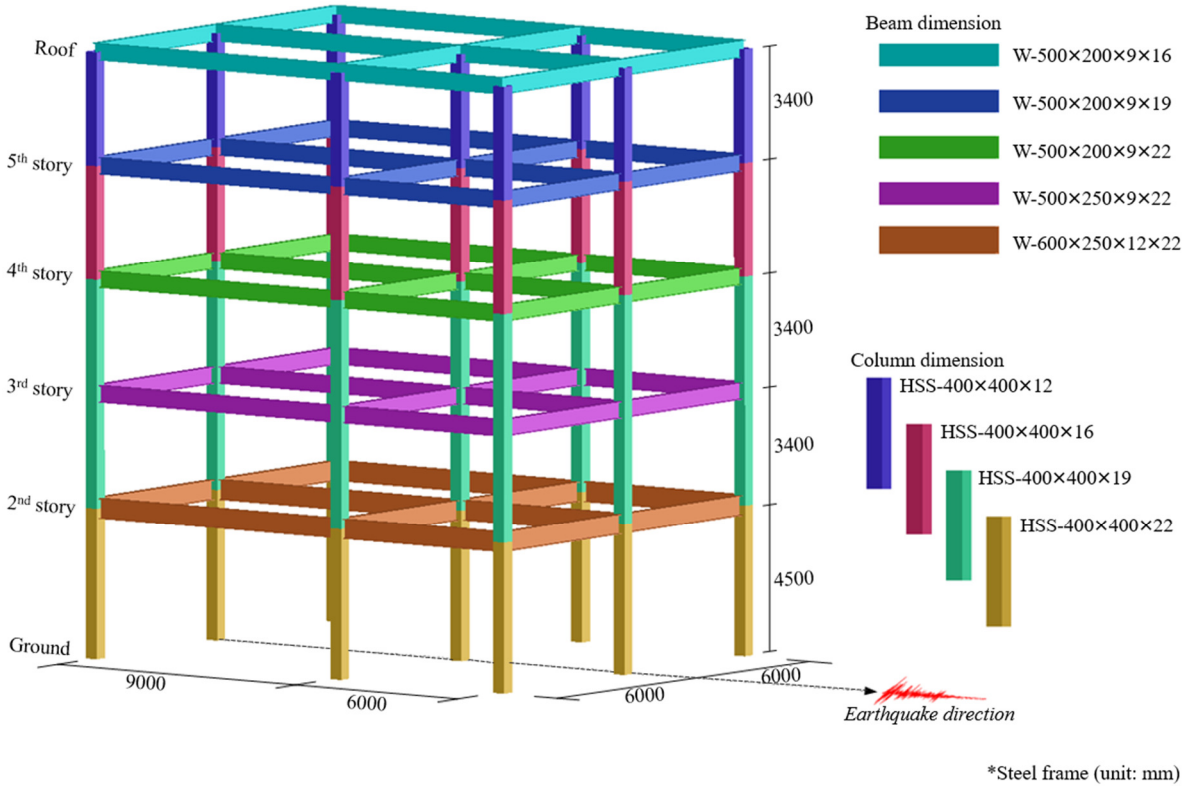

Fig. 1 The building prototype

The ground motion used in this study was the 1940 El Centro seismic wave with a north-south (N-S) orientation. This seismic wave's time history dynamic analysis was applied to the building prototype. The peak ground acceleration (PGA) of the component was 342 gals (cm/s^2), and the time history of the seismic wave is shown in Fig. 2.

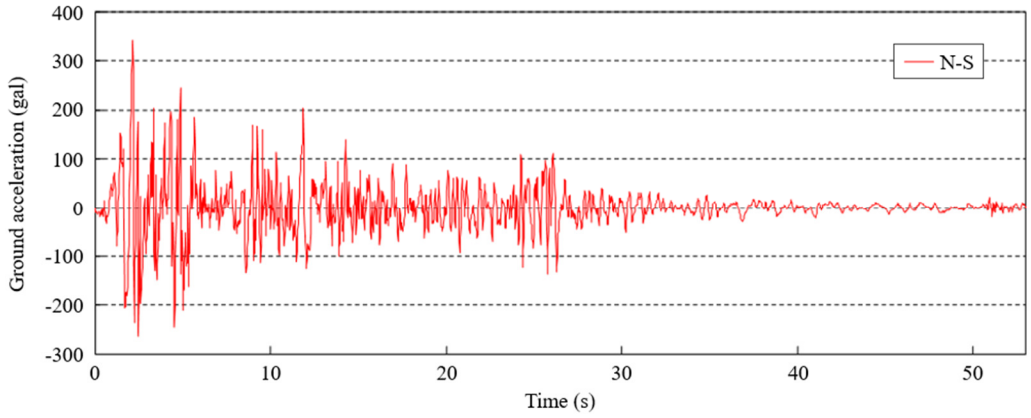

Fig. 2 The time history of the N-S component of the El Centro seismic wave

3. Analyses Tool and Verification

This section provides the basic knowledge of m-SIL as an analysis tool that contains the theory of time history nonlinear dynamic analysis and calculation of the SIL value. The verification of the analysis tool is described in the validation results of SIL calculation using three different ground motions and compared to the public-released seismic intensity by the JMA.

3.1. Time history nonlinear dynamic analysis

The response of building structures during earthquakes experiences some complex behaviors that have to be modeled numerically to understand the structural responses and behaviors. The time history nonlinear dynamic analysis [21] with elastic material assumption is adopted in this study to fully represent the seismic response of the building structure, as given in the equation of motion:

$$M\ddot{u} + C\dot{u} + Ku = P_{eff} \tag{1}$$

here, M, C, and K are the mass, damping, and stiffness of the building structure, respectively. The horizontal displacement u, velocity $\dot{u}$, and acceleration $\dot{u}$ are the responses of the building structure. The dot represents differentiation with respect to time t. For the ground motion analysis, the effective earthquake force P_{eff} which produced the dynamic response of the building structure results from the inertia-force of the structure as,

$$P_{eff} = -M\ddot{u}_g \tag{2}$$

$$M\ddot{u} + C\dot{u} + Ku = -M\ddot{u}_g \tag{3}$$

where the minus sign shows that the inertia force is acting on the building structure in the opposite direction of the ground motion. In this study, STRAND7 [22] is used to do all of the time history dynamic analysis of the building structure. The STRAND7 comes with extensive verifications and validation examples.

Newmark's method [23] is a numerical integration technique used to solve the dynamic analysis of building structures subjected to ground motion. The method is commonly used in finite element analysis software to model dynamic systems of building structures. Consider a linear acceleration system, the Newmark's method without iteration can solve the responses of a building structure due to ground motion by using the following formulae for each time step i of displacement, velocity, and acceleration formulations at the time i.

$$u_{i+1} = \frac{\hat{P}_{i+1}}{\hat{K}} \tag{4}$$

$$\dot{u}_{i+1} = \frac{\gamma}{\beta\Delta t}\left(u_{i+1} - u_i\right) + \left(1 - \frac{\gamma}{\beta}\right)\dot{u}_i + \Delta t\left(1 - \frac{\gamma}{2\beta}\right)\ddot{u}_i \tag{5}$$

$$\dot{u}_{i+1} = \frac{1}{\beta\Delta t^2}\left(u_{i+1} - u_i\right) - \frac{1}{\beta\Delta t}\dot{u}_i - \left(\frac{1}{2\beta} - 1\right)\ddot{u}_i \tag{6}$$

where the initial conditions for the response acceleration at time $i = 0$ are given by:

$$\hat{P}_{i+1} = P_{i+1} + A_1 u_i + A_2 \dot{u}_i + A_3 \ddot{u}_i \tag{7}$$

$$\hat{K} = K + A_1 \tag{8}$$

$$A_1 = \frac{1}{\beta\Delta t^2}M + \frac{\gamma}{\beta\Delta t}C \tag{9}$$

$$A_2 = \frac{1}{\beta\Delta t}M + \left(\frac{\gamma}{\beta} - 1\right)C \tag{10}$$

$$A_3 = \left(\frac{1}{2\beta} - 1\right)M + \Delta t\left(\frac{\gamma}{2\beta} - 1\right)C \tag{11}$$

$$\ddot{u}_{i=0} = \frac{-M\ddot{u}_{g,i=0} - C\dot{u}_{i=0} - Ku_{i=0}}{M} \tag{12}$$

In the linear acceleration assumption of Newmark's method, the parameters β and γ play crucial roles in stability and accuracy. If the time step Δt for the dynamic analysis is shorter than the period time of the building structure T_n as given by the formula below, then, in the linear acceleration of Newmark's method the parameter $\beta = 1/6$ and $\gamma = 1/2$ will give stable and accurate results.

$$\frac{\Delta t}{T_n} \leq 0.551 \tag{13}$$

3.2. Calculation of the SIL value

The procedure for computing the m-SIL value of the JMA intensity scale was presented in Shabestari [19]. For clarity, a brief explanation is presented. First, the fast Fourier transform (FFT) is applied to each of the three-component accelerations recorded in the frequency domain of the ground responses [24]. The bandpass filters given in the formula below are then applied to the frequency domain of the three-component accelerations. After the filters are applied, the frequency domain's accelerations are transformed back to the time domain. The normalized vectored composition of the three components is used to calculate the amplitude of the acceleration. The intensity is automatically calculated using three-component ground acceleration records after the application of a band pass filter [19], as follows:

$$\lambda = \lambda_1 \times \lambda_2 \times \lambda_3 \tag{14}$$

where,

$$\lambda_1 = \sqrt{\frac{1}{f}} \tag{15}$$

$$\lambda_2 = \sqrt{1 + 0.694y^2 + 0.241y^4 + 0.0557y^6 + 0.009664y^8 + 0.00134y^{10} + 0.000155y^{12}} \tag{16}$$

$$\lambda_3 = \sqrt{1 - e^{-8f^3}} \tag{17}$$

with $y = f/10$. Here, f represents the frequency, λ_1 represents the filter on-period effect, λ_2 represents the high-cut filter, and λ_3 represents the low-cut filter.

Using the filtered time-domain acceleration and its acceleration vector, the value of m-SIL can be determined as follows:

$$m\text{-}SIL = 2\log\left(A_{0.3}\right) + 0.94 \tag{18}$$

where, the $A_{0.3}$ is the lowest maximum acceleration of a continuous total duration of 0.3 seconds around the peak acceleration response [25].

Fig. 3 illustrates how to determine the $A_{0.3}$ values. Fig. 3(a) shows the bandpass-filtered absolute acceleration response in the time domain. The dotted line defines the lowest maximum acceleration $A_{0.3}$ of a total continuous 0.3 seconds around the peak acceleration. In the second method, the $A_{0.3}$ can also be determined by plotting the cumulative duration against the vector acceleration, as shown in Fig. 3(b). The lowest maximum acceleration of the $A_{0.3}$ can be determined at the cumulative duration of 0.3 seconds.

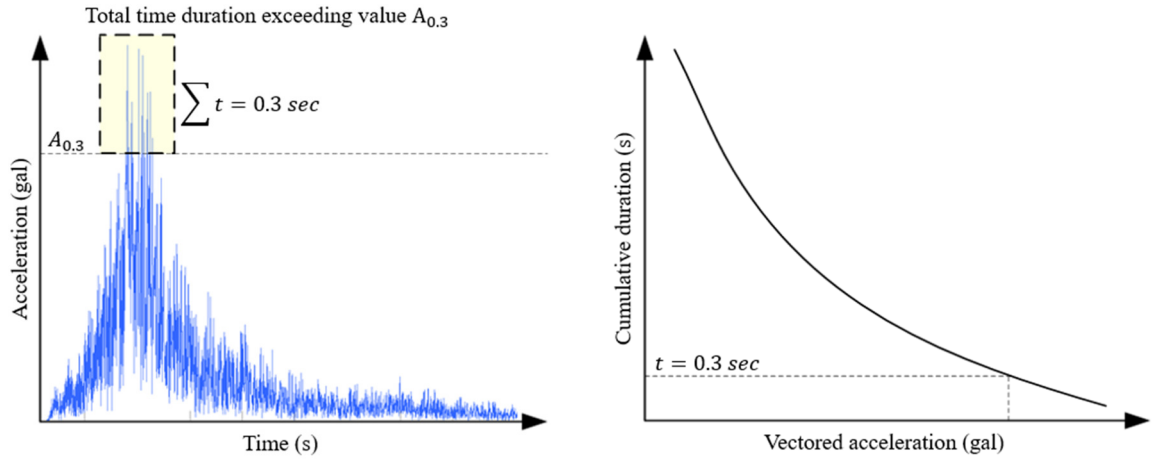

(a) The bandpass-filtered absolute acceleration response

(b) The determination of $A_{0.3}$ by plotting the cumulative duration against the vectored acceleration

Fig. 3 Scheme to determine $A_{0.3}$ value

3.3. Validation of the m-SIL by using real earthquake data

Fig. 4 considers three strong motion earthquakes recorded at three different seismic stations in Japan which were downloaded from the K-NET website to validate m-SIL calculation. The quantitative shaking m-SILs of the ground at the selected seismic stations shown in Fig. 4 are calculated based on the method described in Section 3.2. The results of the m-SILs of the three selected seismic stations are shown in Table 1 below.

In Table 1, the calculation of the m-SILs of three different areas in Japan agreed closely with the Intensity of JMA [26] of ground motions recorded in the selected seismic stations. To conclude, the present quantitative shaking evaluation method is validated.

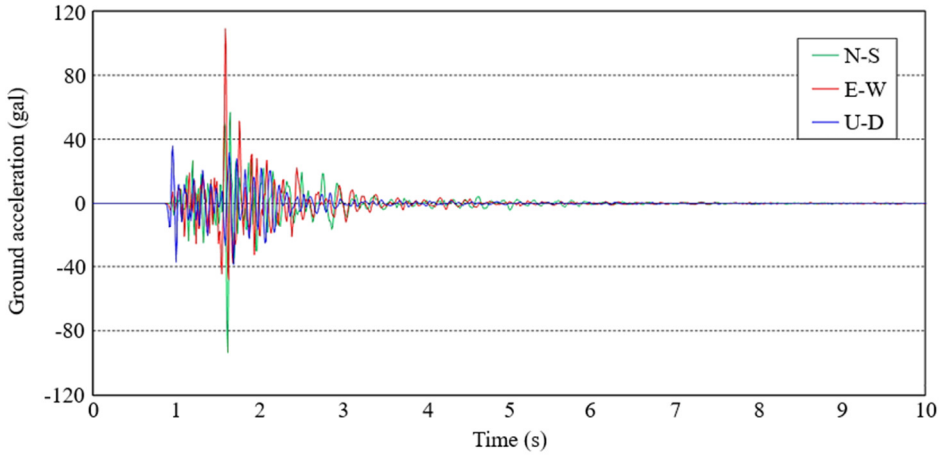

(a) ISK006 seismic station

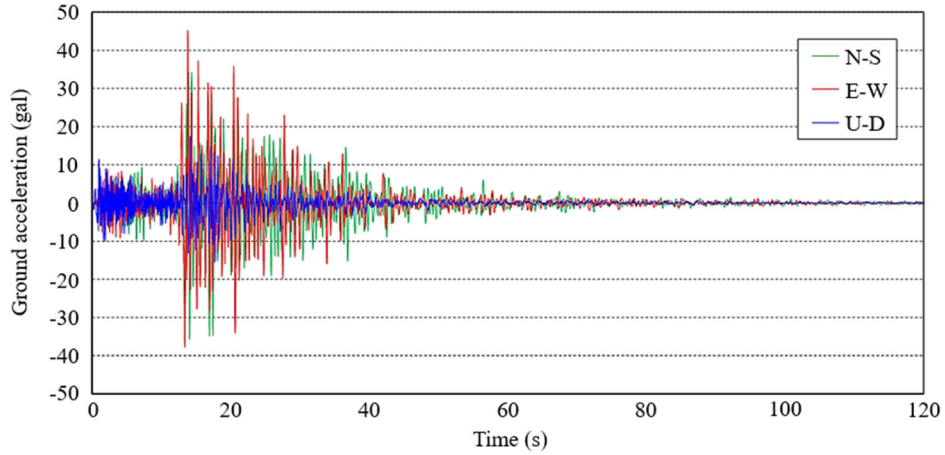

(b) NIG025 seismic station

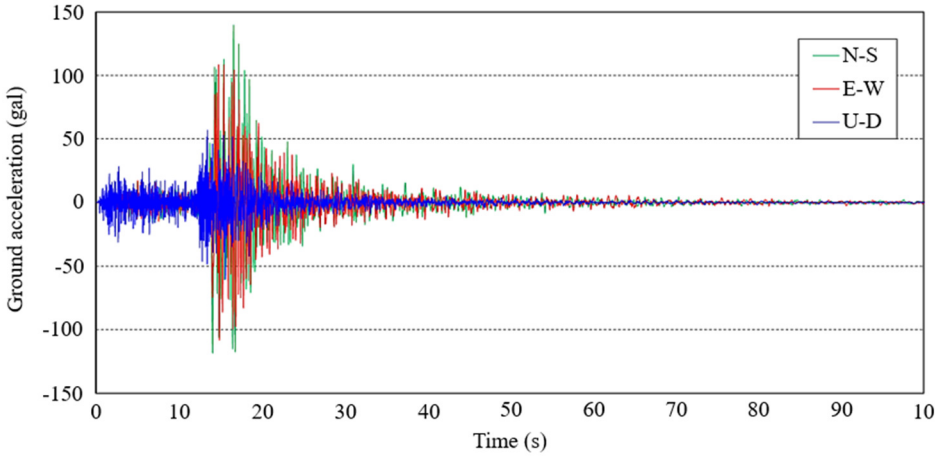

(c) HKD066 seismic station

Fig. 4 Ground motion waves recorded in three different seismic stations in Japan

Table 1 Validation of m-SILs and intensity (JMA) at three seismic stations in Japan

Location	Site code	Latitude (deg)	Longitude (deg)	Depth (km)	Magnitude (Richter)	PGA (gal)	Intensity (JMA)	Epicentral distance (from the source)	m-SIL (JMA)
Ishikawa prefecture	ISK006	37.1 [37.2]	136.7 [136.6]	[10]	[2.8]	93.44	2.6	9 km Date: 2024/05/15 02:49:00	2.54
Niigata prefecture	NIG025	37.2 [37.5]	138.2 [137.3]	[10]	[5.9]	35.76	3.9	90 km Date: 2024/06/03 06:31:00	3.85
Hokkaido	HKD066	43.7 [42.8]	145.1 [145.1]	[63]	[6.0]	108.64	4.7	101 km Date: 2023/02/25 22:27:00	4.64

* Numbers in [ ] show the information of the earthquake source

4. Result and Analyses

The results of this study are categorized according to the model types, which are NA building, BS building, and BI strengthened building. Each model is analyzed to evaluate the seismic performance described by m-SIL, accelerations, and kinetic energy.

4.1. Non-strengthened (NA) building shaking performance

The discussion of the shaking performance of NA buildings is outlined in this section. Evaluation of m-SIL is depicted for every floor to give an early insight into the implementation of SIL on the building's floors. Furthermore, the building's accelerations and kinetic energy evaluation are also explained, especially for the rooftop, which tends to have the biggest value.

4.1.1. m-SIL evaluation

The shaking performance of NA was evaluated, and the results are presented in Table 2, showing that the higher the number of floors, the higher the m-SIL of the building. Fig. 5 demonstrates that the m-SIL values of each floor in the building can be determined by plotting the dominant period values and the maximum accelerations calculated by the JMA SIL equation [25, 27]. This method and sequence were applied to all specimens throughout the study. From Fig. 5, the $A_{0.3}$ is found to be 1,739.9 gals (m-SIL = 6.8). This value is ten times more than that on the ground floor $A_{0.3}$ of the existing building measured to be 164.4 gals (m-SIL = 5.2).

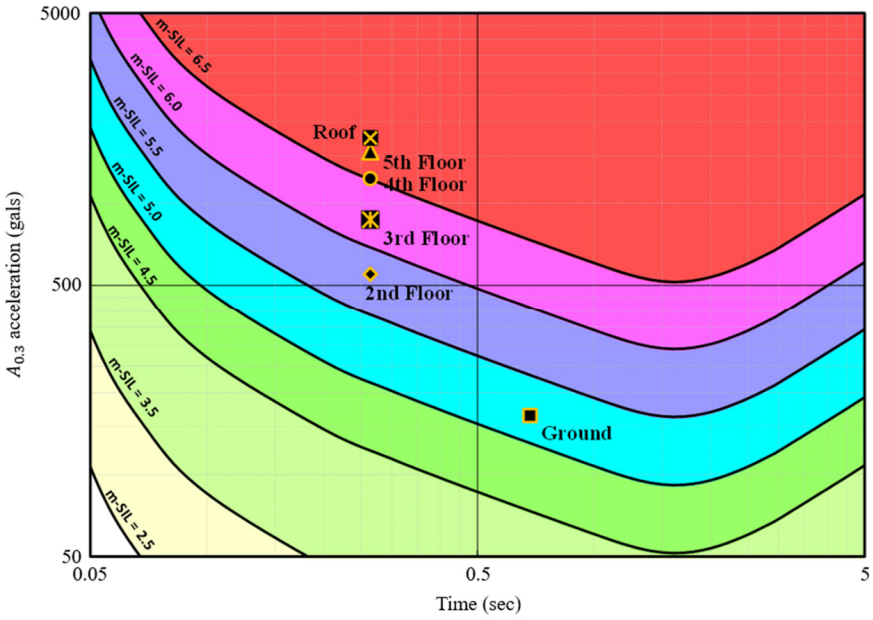

Fig. 5 Graphical representation of m-SIL determination of NA

Table 2 m-SIL and $A_{0.3}$ of NA

Floor	m-SIL	Time (sec) [FFT]	$A_{0.3}$ (gals)	Natural frequencies of building prototype
Roof	6.8	0.2643	1739.9	Mode 1: T = 0.2621 sec Mode 2: T = 0.2173 sec Mode 3: T = 0.1870 sec Mode 4: T = 0.0942 sec ⋮ etc.
5	6.7	0.2643	1550.7	
4	6.5	0.2643	1231.8	
3	6.2	0.2643	872.0	
2	5.8	0.2643	550.2	
Ground	5.2	0.6836	164.4	

4.1.2. Accelerations and kinetic energy evaluation

The kinetic energy equation is written as seen in the formula below. This calculation is used to evaluate the effectiveness of several methods of shaking reduction in the following sections and shows the need for SIL as an evaluation tool.

$$E_k = \frac{1}{2} m_a v_a^2(t) \tag{19}$$

where E_k is the kinetic energy of a particular floor in the building, m_a the sum of the mass of the floor and half of the height of columns and $v_a(t)$ the velocity of the moving mass at time *t*. The cumulative kinetic energy computed on the roof is 302.7 kJ (SIL = 6.8). The roof's mass is estimated by adding up the weight of the beams and half of the height of the columns on the fifth floor of the building, yielding a total of 12.726,6 kg.

4.2. Bracing-strengthened (BS) building shaking performance

The strengthening of the existing building using bracing was tested by considering the weight and the configuration of the bracing. The m-SIL results of each floor, the roof's response acceleration, and kinetic energy are presented by comparing the values to the NA model results.

4.2.1. m-SIL evaluation

Based on the configuration of bracings, the buildings were distinguished into ten types. Types I-IV included single diagonal bracings with a 9.5% weight-to-building ratio situated between frames A-B as seen in Fig. 6(a). Types V-VIII used singled-bracing bracings with a total 16.3% weight ratio between both frames A-B and B-C (Fig. 6(b)). Finally, type IX consumed 18.9% of bracing with a configuration between frames A-B. In comparison, type X used 32.6% between frames A-B and B-C (Fig. 6(c)). These two types were cross-braced.

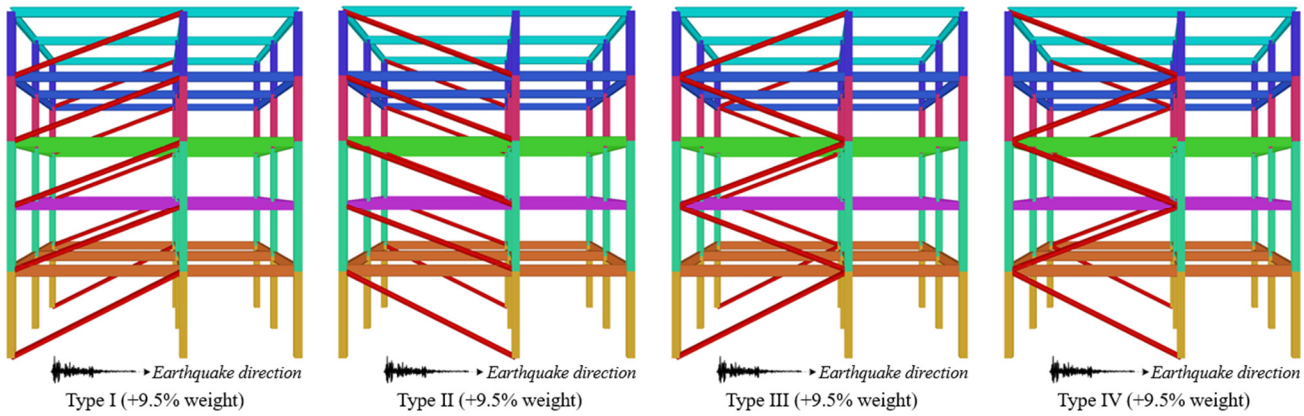

(a) Building models with additional bracing of 9.5% of the total weight

Fig. 6 Bracing-strengthened (BS) building categories

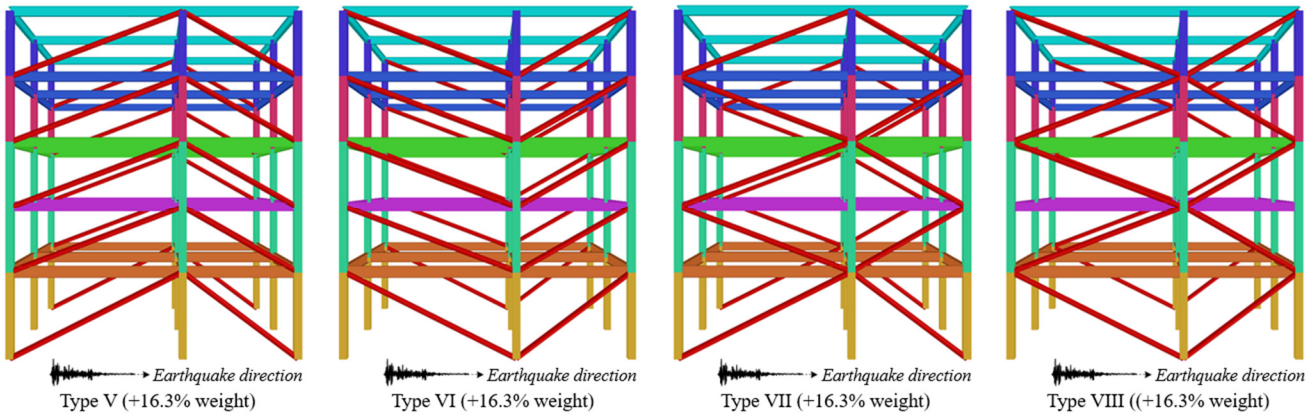

(b) Building models with additional bracing of 16.3% of the total weight

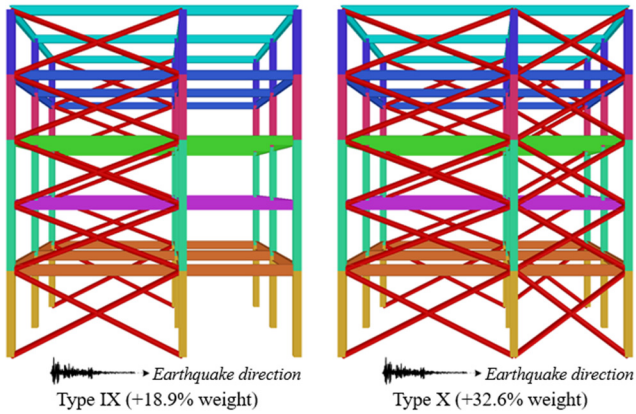

(c) Building models with additional bracing of 18.9% and 32.6% of total weight

Fig. 6 Bracing-strengthened (BS) building categories (continued)

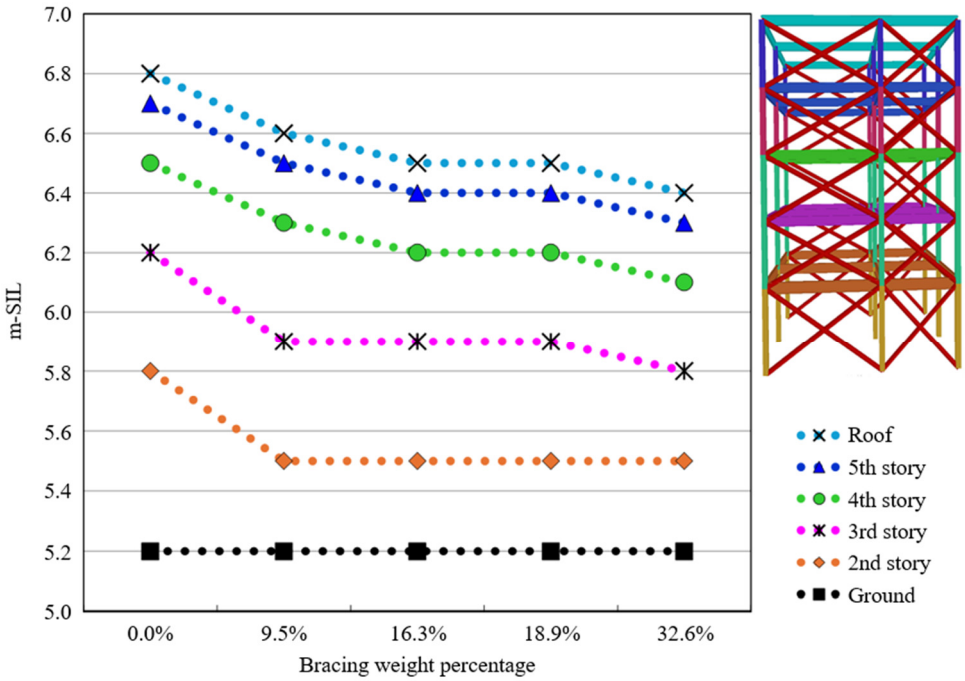

Fig. 7 m-SIL comparison BS to NA as a function of bracing weight ratio

The 9.5% additional bracing in weight ratio (type I-IV) analyses showed that the four strengthening methods produced comparable m-SIL values for each building floor. Analog, the additional 16.3% bracing in weight ratio (type V-VIII) m-SILs were also very closely approaching one another for each floor. The m-SIL of all BS are presented in Table 2. It is concluded that the configuration of bracings for the same weight-to-building ratio did not influence the m-SIL. The analyses demonstrated

that the relative weight of bracings decreased the m-SIL for every floor level (Fig. 7). On average, type (I-IV) resulted in values slightly lower than NA's m-SIL values. The maximum acceleration at each position was calculated using the procedure outlined in the previous section based on the m-SIL values. The m-SIL at the ground is lower than on the roof.

Table 3 also demonstrates that the strengthening methods V-VIII display comparable m-SIL values for each floor in the building, compared to methods I-IV. The results suggest that the addition of 6.8% weight of bracing does not significantly decrease the level of seismic activity on each floor, measuring only approximately 0.1 units in m-SIL values. Given the high cost of materials, these slight reductions in seismic activity are not considered significant enough. Despite this, the strengthening methods Designers may still prefer V-VIII in practice due to a lack of knowledge about the present methodology. Further, Table 3 reveals that the IX-X strengthening methods show limited improvement in m-SIL values for each building floor. Adding either 9.4% (type IX) or 23.1% (type X) weight of bracing only results in a small reduction of 0.3-0.4 on the m-SIL values scale, compared to the I-VIII strengthening methods. The improvement is insignificant.

Table 3 m-SIL for every bracing category

Floor	m-SIL of BS				
	NA	(I-IV)	(V-VIII)	(IX)	(X)
Roof	6.8	6.6	6.5	6.5	6.4
5	6.7	6.5	6.4	6.4	6.3
4	6.5	6.3	6.2	6.2	6.1
3	6.2	5.9	5.9	5.9	5.8
2	5.8	5.5	5.5	5.5	5.5
Ground	5.2	5.2	5.2	5.2	5.2

As an illustration, the m-SIL values of NA and BS type X buildings were obtained by plotting the dominant period values and the maximum accelerations calculated by the JMA SIL equation, which are shown in Fig. 8. Generally, it is shown that the reduction of the m-SIL values from NA to BS type X building for the second floor to the rooftop only gains a level down.

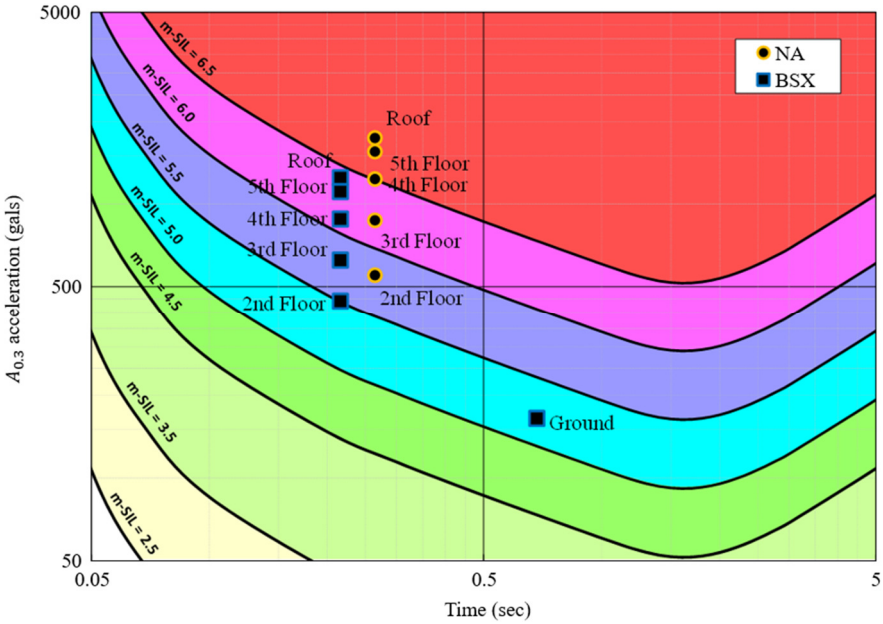

Fig. 8 Graphical representation of m-SIL comparison between NA and BS type X

4.2.2. Accelerations and kinetic energy evaluation

The comparison of the roof's response acceleration before and after reinforcement with bracing type IV as a representative of types I-IV can be seen in Fig. 9(a). It is noteworthy that the response accelerations of the roof before and after strengthening were 1,739.9 gals (m-SIL = 6.8) and 1,564.7 gals (m-SIL = 6.6), respectively, as indicated in Fig. 9(a). This resulted in a decrease in the maximum acceleration by 175.2 gals, which is a reduction of 10.1%. From an energy dissipation perspective,

the cumulative kinetic energies of the roof before and after reinforcement were 302.7 kJ (m-SIL = 6.8) and 103.0 kJ (m-SIL = 6.6), as depicted in Fig. 9(b). The energy dissipated after strengthening was 103.0 kJ, which is 34.0% of the total energy. The high energy dissipation capability of the strengthening method is evident, as it reduced the kinetic energy by nearly 70% from the original unstrengthen building. However, the SIL values in both cases do not indicate a significant improvement in reducing the roof's shaking.

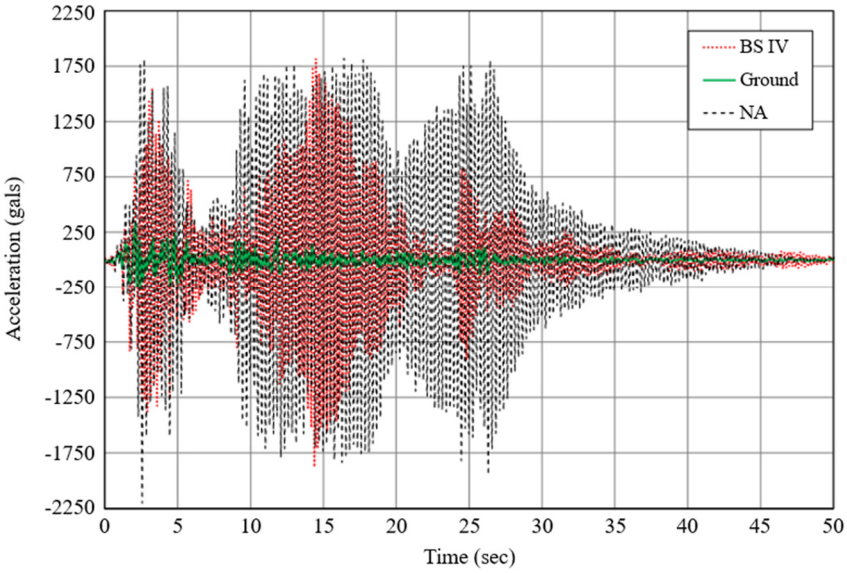

(a) Response acceleration

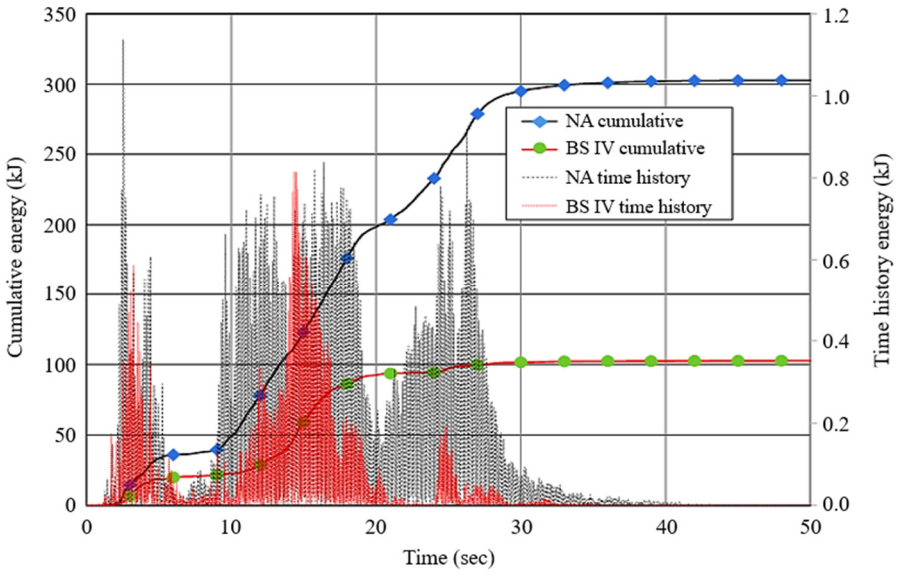

(b) Kinetic energy

Fig. 9 Response accelerations and kinetic energy of the roofs of the bracing-strengthened type IV building

Fig. 10(a) and Fig. 10(b) compare the roof's response acceleration and the kinetic energy before and after being reinforced with bracing type X (the most effective case). Fig. 10(a) shows that the roof's response accelerations before and after strengthening are 1,739.9 gals (m-SIL = 6.8) and 1,245.5 gals (m-SIL = 6.4), respectively. The maximum acceleration has been reduced by 494.4 gals (28.4%). Notably, despite adding a full set of diagonal bracing, the reduction in the maximum response acceleration remains relatively minor. From the energy dissipation perspective, the total amount of kinetic energy absorbed by the roof, before and after reinforcement, was 302.7 kJ (when m-SIL = 6.8) and 100.0 kJ (when m-SIL = 6.4), as shown in Fig. 10(a). The amount of energy absorbed after reinforcement was 100.0 kJ or 67% of the original amount. The high level of energy dissipation suggests that the reinforcement method effectively reduced the kinetic energy of the building by 67%. However, the SIL values in both cases indicate a slight improvement in reducing the roof's vibrations.

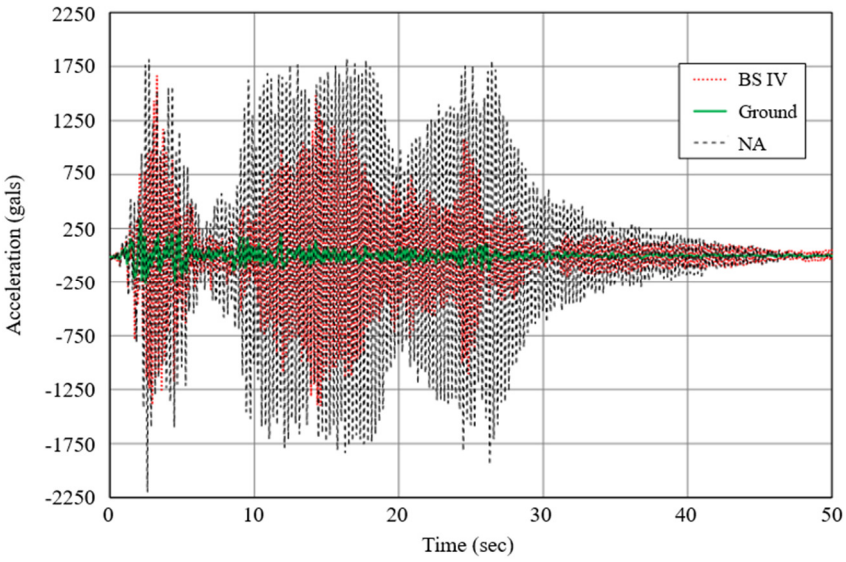

(a) Response acceleration

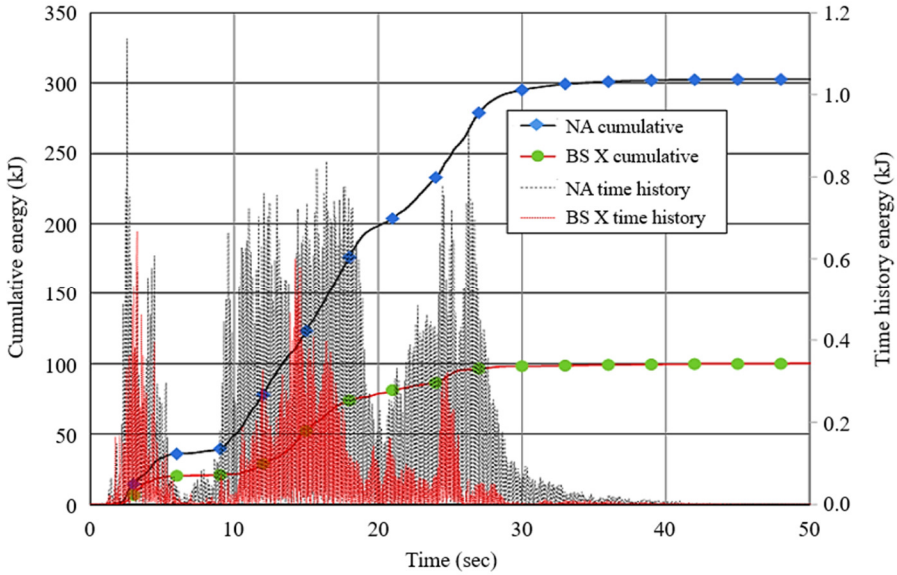

(b) Kinetic energy

Fig. 10 Response accelerations and kinetic energy of the roofs of the bracing-strengthened type X building

The evaluation criteria, based on either maximum acceleration or energy dissipation, can result in varying outcomes for designers to consider when making design decisions. On the other hand, evaluations using SIL provide more consistency. They are simpler to comprehend, as both before and after strengthening scenarios are reduced to a SIL value of 0.4, which does not significantly diminish the building's seismic resistance. Studies on the use of bracing for strengthening purposes have highlighted the advantages of utilizing SIL in assisting designers in making informed decisions, particularly when balancing the requirement for reduced shaking comfort against the cost involved. In reality, many designers are not well-versed in making decisions based solely on the strength criteria outlined in the codes. As observed, even with the densest bracing placement in type X, the level of shaking reduction is not significant. Hence, alternative strengthening methods must be explored to attain the optimal solution.

4.3. Base-isolation (BI) strengthened building shaking performance

This section discusses the process of using BI for vibration control. The implementation is demonstrated through a case study of BI design and implementation and evaluated by computing the SIL for each floor in the building. These SIL values provide crucial information for making informed decisions regarding vibration control. The following examples are presented to demonstrate further BI devices' efficacy in controlling vibrations during strong earthquakes.

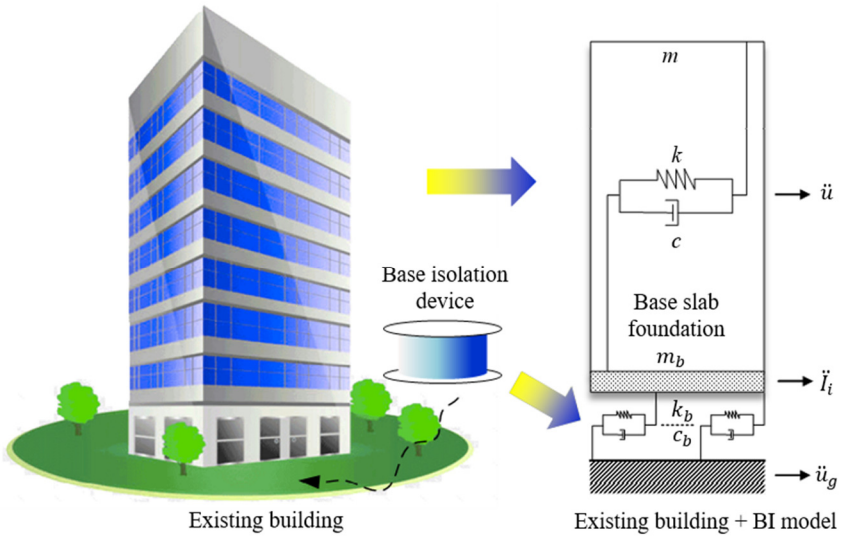

Fig. 11 Illustration of BI seismic control system

The idea of BI is generally illustrated through the use of a two-mass system, as depicted in Fig. 11. The subscript *b* in this figure refers to the BI device. The building structure is simplified as a single lump sum mass system. The dynamic behavior of the building structure connected to a BI device is calculated using the basic equations [21, 28]. The optimal selection for the BI device's natural frequency when designing an optimal BI that reduces building shaking due to ground excitation is given as:

$$\omega_b \ll \omega \tag{20}$$

where ω is the natural circular frequency of the building structure, and ω_b is the natural circular frequency of the slab foundation.

The natural frequency of the BI device is established based on the mass of the slab foundation to which the spring and damper are connected. A combination of springs and elastomeric (lead-rubber) bearings is one of the most commonly used base isolators in practice. The base isolators are installed between the ground and the slab foundation, separating the horizontal movements of the slab and ground, and also show the standard mechanical characteristics of the base isolator foundation, as shown in Fig. 12.

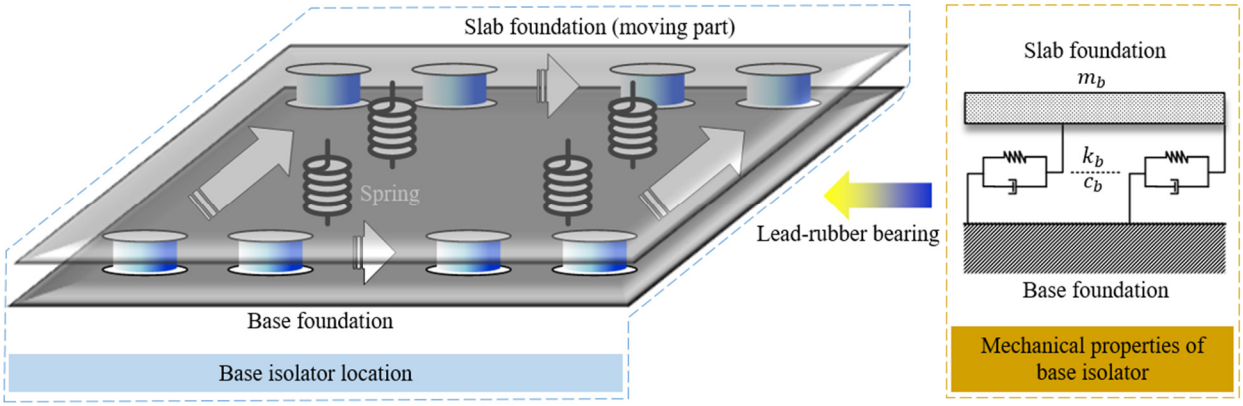

Fig. 12 Base Isolator seismic isolation control system

Six variations in base isolator properties (BI1 to BI6) were considered to have a variation in stiffness (k_{BI}) and damping (c_b). The base floor foundation, considered as the mass of the base isolator, is comprised of a reinforced concrete slab with a compressive strength of 25 MPa and a thickness of 30 cm, resulting in a total mass of 129,600 kg. Table 4 presents the results. Nine of these devices are installed beneath the concrete slab. The natural frequency of the building is compared to that of the base isolator to determine the effectiveness of the design.

Table 4 Varying the mechanical properties of base isolators

Case	Stiffness		Damping		Frequency ratio
	k_{BI} (kN/cm)	% $K_{BUILDING}$	c_b (kN.sec/cm)	ξ_b (%)	ω_b/ω (%)
BI1	2.8170	2.90	15.5331	25.0	2.8
BI2	1.1268	1.50	15.5331	25.0	2.8
BI3	2.8170	2.90	6.9037	100.0	4.2
BI4	1.1268	1.50	0.3452	5.0	1.3
BI5	0.5634	0.58	0.0690	1.0	0.6
BI6	0.1125	0.12	0.0138	0.2	0.3

4.3.1 m-SIL evaluation

Table 5 presents the m-SIL values for the BI1-BI6. The results indicate that using a base isolator can significantly reduce the m-SIL values on the roof, lowering it from 6.8 to 2.3. Despite the cost of materials and maintenance associated with the base isolator, the results demonstrate that optimizing the mechanical properties of the springs and dampers can lead to the greatest reduction in shaking, as evaluated by the SIL criterion.

Table 5 m-SILs as a function of base property isolator variations

Floor	m-SIL						
	NA	BI1	BI2	BI3	BI4	BI5	BI6
Roof	6.8	4.3	4.7	5.3	4.2	3.5	2.3
5	6.7	4.3	4.7	5.3	4.2	3.5	2.3
4	6.5	4.2	4.7	5.2	4.2	3.5	2.2
3	6.2	4.1	4.6	5.2	4.2	3.5	2.2
2	5.8	4.1	4.6	5.1	4.2	3.5	2.2
Ground	5.2	5.2	5.2	5.2	5.2	5.2	5.2

4.3.2. Accelerations and kinetic energy evaluation

For an in-depth evaluation, base isolator BI6 was investigated in detail, as showcased, since the BI6 has the most effective performance. Table 6 and Fig. 13 present the evaluation of BI6 and input ground motion from the 1940 El Centro earthquake. The results demonstrated that the acceleration and m-SIL values generally increase in an upward direction.

Table 6 Results of m-SIL of the building with base isolator type B06

Floor	m-SIL	T (sec) [FFT]	$A_{0.3}$ (gals)	Natural frequencies BI6
Roof	2.3	16.04	27.2	ω_{BI6} = 0.3917 rad/sec T = 16.04 sec
5	2.3	16.04	27.2	
4	2.2	16.04	24.2	
3	2.2	16.04	24.2	
2	2.2	16.04	24.2	
Ground	5.2	0.6836	164.4	

As presented in Table 6, the installation of BI6 generally leads to a significant reduction in the m-SIL values on each floor of the building, compared to the m-SIL values of the NA without the base isolator devices. In practice, to achieve the most effective reduction of shaking in the building by using a base isolator, it is necessary to adjust the natural frequency of vibration of the springs and dampers at a low value (a high period vibration) as given in Eq. (20).

The m-SIL values can be used to calculate the acceleration at each position by following the procedure outlined in Section 3.2. By plotting the dominant period and acceleration values on SIL graphs, it can be observed that the shaking intensity on each floor in the building (with m-SIL values ranging from 2.2 to 2.3) is relatively low compared to ground level (as shown in Fig. 13).

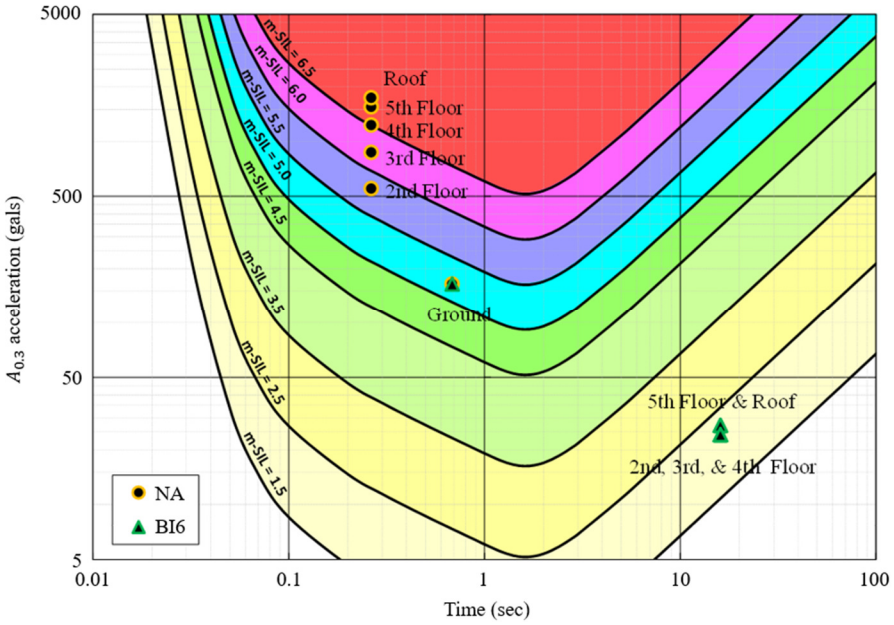

Fig. 13 SIL of the BI6

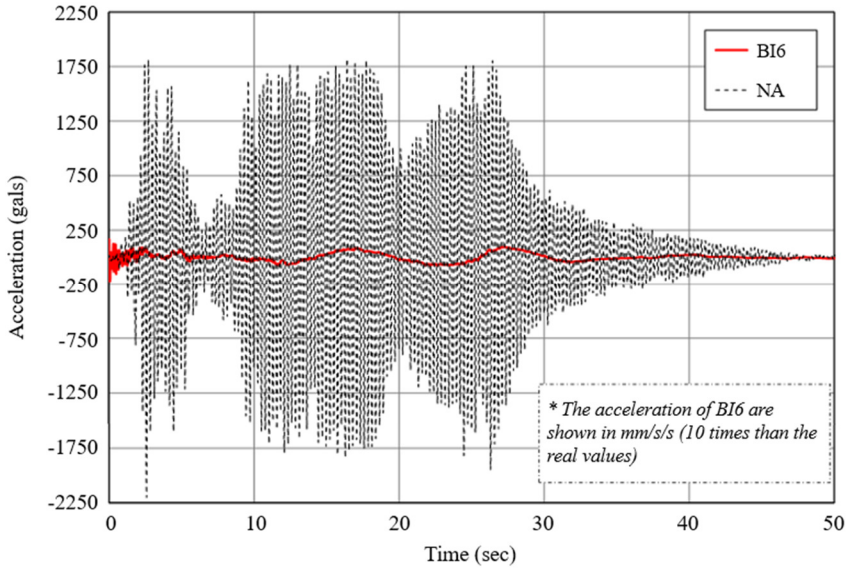

(a) Accelerations of the roof compared to NA

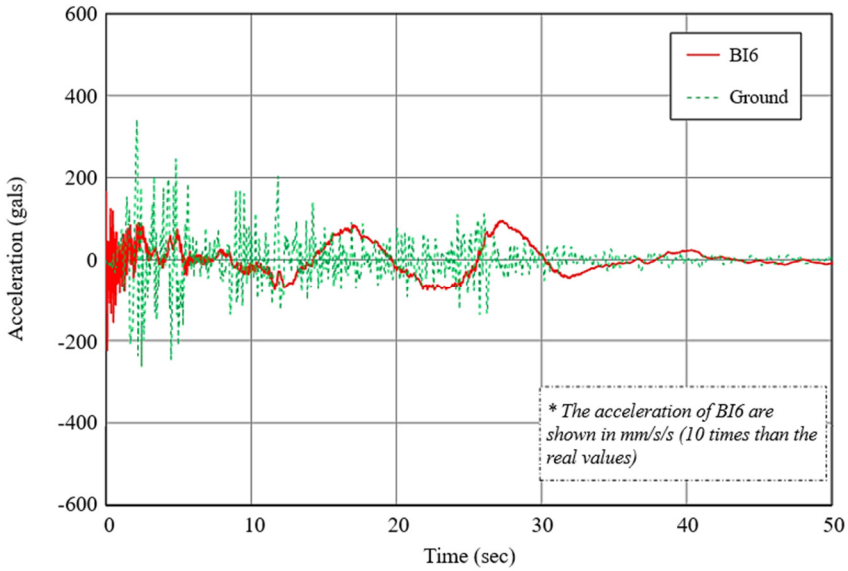

(b) Accelerations of the roof compared to ground level

Fig. 14 Acceleration response comparison of BI6 roof to NA and ground level

The effect of installing base isolator type BI6 (the most effective one) on the response acceleration of the roof is depicted in Fig. 14. Fig. 14(a) shows the maximum response acceleration of the roof before and after the installation of base isolator type BI6; 1,739.9 gals (m-SIL = 6.8) and 27.2 gals (m-SIL = 2.3), respectively. This means that the maximum response acceleration was reduced by 1,712.7 gals (98.4%) after installing the base isolator. This reduction is much higher than that from the BS model. The SIL value was also reduced by four levels, from 6.8 to 2.3. It is important to note that the base isolator decreases the maximum response acceleration of the roof and the SIL value simultaneously.

The reduction in kinetic energy of the roof after installing base isolator type BI6 is substantial, as demonstrated in Fig. 15. The cumulative kinetic energy of the roof before installation was 302.7 kJ (m-SIL = 6.8). In contrast, after installation, it was reduced to 9.1 kJ (m-SIL = 2.3), representing a decrease of 293.6 kJ or 97.0%. The base isolator, particularly type BI6, is highly effective in dissipating almost all of the kinetic energy, thereby preventing the energy from the ground motion caused by an earthquake from being transmitted into the building. The dampers of the base isolator are crucial in dissipating energy.

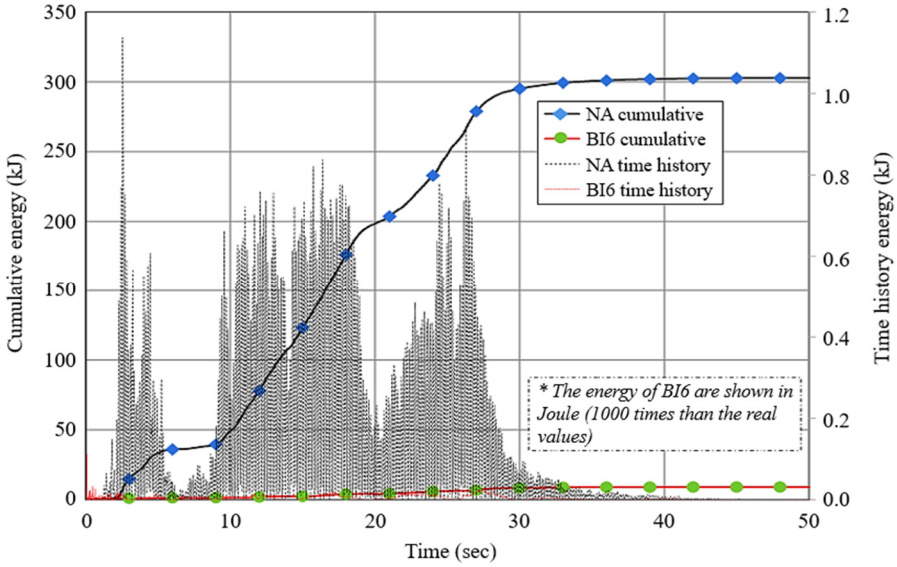

Fig. 15 Kinetic energy of the roofs of the buildings

The study of base isolators as seismic protection highlights the significance of SIL as an evaluation tool in helping designers make informed decisions. Many designers cannot decide solely based on strength criteria in real-world design, as outlined in the seismic design codes. Base isolator manufacturers typically rely on experience in design. However, there is no clear method for evaluating the effectiveness of the installed base isolator. As such, the use of shaking evaluation based on SIL, with its quantifiable descriptions of shaking intensity, is highly recommended for practical design purposes.

5. Summary and Conclusions

This study demonstrates the efficacy of SIL as an evaluation tool for assessing the seismic aspect of buildings, contrasting with traditional evaluation criteria such as maximum acceleration or energy dissipation, SIL offers consistency and simplicity, facilitating informed design decisions. There are two key findings obtained from this study:

(1) The significance of SIL as an evaluation tool: Although both bracing and base isolators demonstrate significant reductions in maximum acceleration (28.4% for bracing and 98.4% for base isolators) and energy dissipation (67.0% for bracing and 97.0% for base isolators), the corresponding decrease in SIL values reveals nuanced insights. Despite the apparent reduction in structural response metrics, base isolators exhibit a more substantial SIL decrease (4.5 levels) compared to bracing (0.4 levels). This disparity underscores the importance of SIL as a comprehensive evaluation tool for building seismic behavior. While traditional metrics may indicate significant improvements in structural performance, the SIL

value provides a more nuanced understanding of the building's resilience. Therefore, the comprehensive assessment facilitated by SIL reaffirms its significance as an invaluable tool in evaluating the seismic behavior of buildings, guiding informed decision-making in seismic design and reinforcement strategies.

(2) Performance comparison of strengthening methods: Comparing the two methods, the BI system emerges as the safer option, significantly reducing both maximum acceleration (98.4%) and dissipated energy (97.0%). In contrast, bracing shows minimal change in the SIL value (only a 0.4 level decrease), whereas the base isolator offers a substantial decrease in m-SIL (up to a 4.5 level decrease), enhancing overall seismic resilience. These findings contribute to the ongoing discourse on seismic engineering, providing actionable insights for architects, engineers, and policymakers striving to enhance the seismic resilience of built environments.

Acknowledgment

The authors gratefully acknowledge the financial support of the research funding by the Directorate of Research, Technology and Community Service, Directorate General of Higher Education, Research and Technology, Ministry of Education, Culture, Research and Technology, the Republic of Indonesia through the grant number 601-66/UN7.D2/PP/VI/2024 and The Universitas Atma Jaya Yogyakarta for their funding, through grant nr. 578/In/HIBAH-PKSI/2022.

Nomenclature

BI	Base-isolation or base-isolated	$k_{BUILDING}$	The stiffness parameter of the building structure
BS	Bracing-strengthened, to denote a structure strengthened by bracing	M	Mass matrix of the building structure
CSM	Capacity spectrum method	m_a	The story mass
FFT	Fast Fourier transform	P_{eff}	The effective earthquake force
JMA	Japan Meteorological Agency	T_n	The period time of the building structure
MR	Magnetorheological	u	Displacement response vector
m-SIL	measured or calculated seismic intensity level	$\dot{u}$	Velocity response vector
NA	Not any, to denote a structure without strengthening	$\ddot{u}$	Acceleration response vector
PGA	Peak ground acceleration	$\ddot{u}_g$	The ground motion acceleration
SIL	Seismic intensity level	v_a	The velocity of the moving mass
TLD	Tuned liquid damper	Δt	Time step
TMD	Tuned mass damper	β	Beta value in Newmark method
$A_{0.3}$	The cumulative acceleration in 0.3 second	γ	Gamma value in Newmark method
C	Damping matrix of building structure	λ_1	The filter on-period effect
c_b	The damping parameter of base-isolator	λ_2	The high-cut filter
E_k	Kinetic energy	λ_3	The low-cut filter
f	The frequency	ω	Natural circular frequency of building structure
K	Stiffness matrix of building structure	ω_b	Natural circular frequency of foundation
k_b or k_{BI}	The stiffness parameter of base-isolator	ξ_b	Damping ratio

Conflicts of Interest

The authors declare no conflict of interest.

References

[1] G. Xu, T. Guo, A. Li, H. Zhang, K. Wang, J. Xu, et al., "Seismic Resilience Enhancement for Building Structures: A Comprehensive Review and Outlook," Structures, vol. 59, article no. 105738, January 2024.

[2] A. Singh and S. Palissery, "Preferred Seismic Performance Attainment in Important Buildings," Engineering Failure Analysis, vol. 158, article no. 107952, April 2024.

[3] R. Siano, A. Fatnassi, F. V. De Maio, P. Basso, and M. Cademartori, "Seismic Vulnerability Assessment and Retrofitting Design of Italian Public Buildings," Procedia Structural Integrity, vol. 44, pp. 1038-1044, 2023.
[4] M. H. El Ouni, M. Abdeddaim, S. Elias, and N. B. Kahla, "Review of Vibration Control Strategies of High-Rise Buildings," Sensors, vol. 22, no. 21, article no. 8581, November 2022.
[5] M. Bhandari, S. D. Bharti, M. K. Shrimali, and T. K. Datta, "The Numerical Study of Base-Isolated Buildings Under Near-Field and Far-Field Earthquakes," Journal of Earthquake Engineering, vol. 22, no. 6, pp. 989-1007, 2018.
[6] M. Bhandari, S. D. Bharti, M. K. Shrimali, and T. K. Datta, "Assessment of Proposed Lateral Load Patterns in Pushover Analysis for Base-Isolated Frames," Engineering Structures, vol. 175, pp. 531-548, November 2018.
[7] M. Bhandari, S. D. Bharti, M. K. Shrimali, and T. K. Datta, "Seismic Fragility Analysis of Base-Isolated Building Frames Excited by Near- and Far-Field Earthquakes," Journal of Performance of Constructed Facilities, vol. 33, no. 3, article no. 04019029, June 2019.
[8] M. Bhandari, S. D. Bharti, M. K. Shrimali, and T. K. Datta, "Applicability of Capacity Spectrum Method for Base-Isolated Building Frames at Different Performance Points," Journal of Earthquake Engineering, vol. 25, no. 2, pp. 270-299, 2021.
[9] M. Abdeddaim, S. Djerouni, A. Ounis, B. Athamnia, and E. N. Farsangi, "Optimal Design of Magnetorheological Damper for Seismic Response Reduction of Base-Isolated Structures Considering Soil-Structure Interaction," Structures, vol. 38, pp. 733-752, April 2022.
[10] F. Guo, Y. Dong, H. Tian, X. Zhang, and Q. Su, "Structural Seismic Response Prediction Based on Convolutional Neural Networks," Vibroengineering Procedia, vol. 51, pp. 56-62, October 2023.
[11] M. Erdik, Ö. Ülker, B. Şadan, and C. Tüzün, "Seismic Isolation Code Developments and Significant Applications in Turkey," Soil Dynamics and Earthquake Engineering, vol. 115, pp. 413-437, December 2018.
[12] P. Fajfar, "Analysis in Seismic Provisions for Buildings: Past, Present and Future," Recent Advances in Earthquake Engineering in Europe: 16th European Conference on Earthquake Engineering-Thessaloniki 2018, pp. 1-49, June 2018.
[13] B. S. Gan, Design Concepts for Seismic-Resistant Buildings: Quantitative Shaking Evaluations, Newcastle upon Tyne: Cambridge Scholars Publishing, 2023.
[14] E. Nouchi, N. G. Wariyatno, A. L. Han, and B. S. Gan, "Comfort-Based Criteria for Evaluating Seismic Strengthening Performance of Building," IOP Conference Series: Earth and Environmental Science, vol. 1195, article no. 012002, 2023.
[15] H. Wu, "Characteristics of Strong Ground Motions and Fragility Curves of Buildings During the 2011 off the Pacific Coast of Tohoku Earthquake," Ph.D. dissertation, Department of Civil Engineering, Aichi Institute of Technology, Toyota, September 2013.
[16] T. Ishikawa, M. Yoshimi, K. Isobe, and S. Yokohama, "Reconnaissance Report on Geotechnical Damage Caused by 2018 Hokkaido Eastern Iburi Earthquake With JMA Seismic Intensity 7," Soils and Foundations, vol. 61, no. 4, pp. 1151-1171, August 2021.
[17] T. Mukunoki, K. Kasama, S. Murakami, H. Ikemi, R. Ishikura, T. Fujikawa, et al., "Reconnaissance Report on Geotechnical Damage Caused by an Earthquake With JMA Seismic Intensity 7 Twice in 28 h, Kumamoto, Japan," Soils and Foundations, vol. 56, no. 6, pp. 947-964, December 2016.
[18] N. G. Wariyatno, H. A. Lie, F. P. Hsiao, and B. S. Gan, "Design Philosophy for Buildings' Comfort-Level Performance," Advances in Technology Innovation, vol. 6, no. 3, pp. 157-168, July 2021.
[19] K. T. Shabestari, "Attenuation Relationship of JMA Seismic Intensity Using Recent JMA Records," Proceedings of the 10th Earthquake Engineering Symposium, pp. 529-534, November 1998.
[20] K. Kasai, S. Motoyui, H. Ito, H. Ozaki, M. Ishii, K. Kajiwara, et al., "Full-Scale Tests of Passively-Controlled 5-Story Steel Building Using E-Defense Shake Table Part 1: Test Concept, Method, and Building Specimen," Behaviour of Steel Structures in Seismic Areas, 1st ed, London: CRC Press, pp. 29-36, 2009.
[21] A. K. Chopra, Dynamics of Structures : Theory and Applications to Earthquake Engineering. Fifth Edition in SI Units, Global ed. Harlow, United Kingdom: Pearson Education Limited, 2020.
[22] Strand7 Pty Ltd., "Strand7 Software: Overview" https://www.strand7.com/html/brochure.htm, June 06, 2021.
[23] N. M. Newmark, "A Method of Computation for Structural Dynamics," Journal of the Engineering Mechanics Division, vol. 85, no. 3, pp. 67-94, July 1959.
[24] V. Y. Sokolov, "Seismic Intensity and Fourier Acceleration Spectra: Revised Relationship," Earthquake Spectra, vol. 18, no. 1, pp. 161-187, February 2002.
[25] H. Kawasumi, "Measures of Earthquake Danger and Expectancy of Maximum Intensity Throughout Japan As Inferred From Seismic Activity in Historical Time," Bulletin of the Earthquake Research Institute, vol. 21, pp. 469-481, 1951.
[26] Strong-motion Seismograph Networks (K-NET, KiK-net), https://www.kyoshin.bosai.go.jp/, June 19, 2024.
[27] A. Japan Meteorological, "Method of Calculating Measured Seismic Intensity," https://www.data.jma.go.jp/eqev/data/kyoshin/kaisetsu/calc_sindo.html, February 11, 2023.
[28] F. Naeim and J. M. Kelly, Design of Seismic Isolated Structures: From Theory to Practice, New York: John Wiley, 1999.

Copyright© by the authors. Licensee TAETI, Taiwan. This article is an open-access article distributed under the terms and conditions of the Creative Commons Attribution (CC BY-NC) license (http://creativecommons.org/licenses/by/4.0/).